npj | clean water

Article

Published in partnership with King Fahd University of Petroleum & Minerals

https://doi.org/10.1038/s41545-025-00439-5

Tailoring microbial redox with alternating current for efficient mineralization of refractory organic nitrogen compounds in wastewater

Ye Yuan[1,7], Xucui Qian[1,7], Lulu Zhang[1], Wanxin Yin[1], Tianming Chen[1], Zhaoxia Li[1], Cheng Ding[1], Bo Wang[2,3], Bin Liang[4], Aijie Wang[4], Yang Liu[5] ✉ & Fan Chen[1,6] ✉

Traditional biological wastewater treatment struggles to efficiently remove refractory organic nitrogen compounds (RONCs). This study demonstrates the potential of alternating current (AC)-driven bioelectrodes for deep mineralization of nitrobenzene (NB) by coupling in situ reduction and oxidation reactions. Sine-wave AC bioelectrodes overcome the limitations of direct current (DC) systems, achieving 97.6% NB reduction, 90.9% intermediate mineralization, and 80.8% total nitrogen removal while reducing energy consumption by 22.3%. AC stimulation enhances biofilm formation and bidirectional electrocatalytic activity, leading to higher biomass and electron utilization efficiency. Multi-omics analysis shows enrichment of functional microbial consortia involved in NB reduction, aromatic compound oxidation, ammonia oxidation, nitrate/nitrite reduction, and electron transfer, with upregulated enzyme gene expression. Carbon metabolites from catechol meta-cleavage support nitro-reduction, denitrification, and cell viability without external carbon sources. Nitrification-denitrification is the primary pathway for inorganic nitrogen removal. This AC bioelectrode offers an efficient, low-carbon solution for RONC mineralization in wastewater.

Nitroaromatic compounds (NACs), a crucial subset of refractory organic nitrogen compounds (RONCs), encompass nearly 65,000 variants extensively used in industries such as pharmaceuticals, dyes, and pesticides, resulting in substantial volumes of RONC-laden wastewater[1]. Characterized by at least one nitro group ($-NO_2$) on the aromatic ring, these compounds are challenging to biomineralize due to their stable π-conjugated structures and strong electron-withdrawing groups, often surpassing the effluent standards for carbon and nitrogen removal in conventional wastewater treatment plants (WWTPs)[2]. Due to their persistence, bioaccumulation, acute toxicity, mutagenicity, and carcinogenicity, NACs pose severe environmental and health risks[3].Therefore, developing effective methodologies for their complete elimination from wastewater is of paramount importance.

Nitro-amination and ammonification are crucial steps in the biotransformation of NACs into ammonia (NH_4^+), achievable through microbial redox processes. Anaerobic microbial reduction is typically used to diminish the electron-withdrawing properties of NACs by converting nitro groups into amino groups ($-NH_2$), resulting in aromatic amines that significantly reduce toxicity and enhance biodegradability[4]. Additionally, these aromatic amine intermediates require subsequent cleavage and complete mineralization via microbial oxidation processes[5]. Following the cleavage of C–N bonds and conversion of NACs into NH_4^+, this inorganic nitrogen must be eliminated via nitrification and denitrification processes[6]. While sequential aerobic-anaerobic processes can mineralize NACs and achieve synergistic carbon and nitrogen removal, their effectiveness is limited by electron availability during the anaerobic phase and the energy-intensive aeration in the aerobic phase, which consumes up to 90% of WWTP electricity[3,7]. Moreover, multiple treatment units and complex control systems increase both capital and operational expenses. The

[1]School of Environmental Science and Engineering, Yancheng Institute of Technology, Yancheng, 224051, P.R. China. [2]Department of Food Science, Aarhus University, 8200 Aarhus N, Denmark. [3]Center for Electromicrobiology, Section for Microbiology, Department of Biology, Aarhus University, 8000 Aarhus C, Denmark. [4]State Key Laboratory of Urban Water Resource and Environment, School of Civil and Environmental Engineering, Harbin Institute of Technology Shenzhen, Shenzhen, 518055, P.R. China. [5]College of Eco-Environmental Engineering, Qinghai University, Xining, 810016, P.R. China. [6]School of Ecology and Environment, Northwestern Polytechnical University, Xi'an, 710129, P.R. China. [7]These authors contributed equally: Ye Yuan, Xucui Qian.
✉e-mail: ecosea@outlook.com; chenfanhit@163.com

application of solid electrodes as electron donors and acceptors for microbial reduction and oxidation has emerged as a sustainable, controllable, and low-carbon alternative[8]. These bioelectrodes regulate microbial respiratory pathways and boost metabolic activity, significantly enhancing the biotransformation of NACs[9].

Direct current (DC) is routinely employed to drive bioelectrodes for cathodic reduction and anodic oxidation. In DC bioelectrode systems, cathode and anode reactions are spatially separated, and efficient cooperation between them is crucial for the simultaneous reduction of NACs and oxidation of aromatic amines[5]. However, matching these reactions through control of electrochemical conditions, electrode distance, and hydraulic parameters is challenging. In addition, cathodic and anodic biofilms exhibit unique electron transfer and film formation properties, necessitating specific culture conditions for optimal performance[10]. Furthermore, the continuous electron loss inherent in DC systems leads to electrode oxidation and corrosion, hindering current transmission and shortening electrode lifespan[11,12]. Additionally, DC electrochemical systems can produce highly reactive byproducts such as •OH, O_3, H_2O_2, and Cl_2, which can negatively affect microbial activity and biological electrocatalytic performance[13]. Recently, alternating current (AC)-driven bioelectrodes, undergoing microbial redox over time and enabling in situ coupling of microbial reduction and oxidation, have shown significant potential in enhancing the biotransformation of refractory organic pollutants[14]. Additionally, the broad potential range of AC bioelectrodes can activate diverse microbial reactions, enhancing biosystem efficiency[13]. AC stimulation promotes electroactive biofilms with bidirectional electron transfer while minimizing harmful byproducts and electrode corrosion by maintaining a zero net charge[15]. This approach simplifies operations, expands the electrochemical reaction zone, and potentially overcomes mass and electron transfer inefficiencies present in traditional DC bioelectrode. Despite the potential of AC bioelectrodes to enhance RONC degradation, the mechanisms underlying carbon and nitrogen reduction during this process remain unclear. The effectiveness of AC bioelectrodes in achieving deep mineralization of RONCs is still unexplored. Moreover, significant knowledge gaps persist regarding how AC regulates microbial redox processes, biofilm growth, and the composition and functionality of electromicrobiome.

In this study, AC bioelectrodes were developed to regulate microbial redox processes for the efficient mineralization of RONCs (e.g., nitrobenzene (NB)) in wastewater. The study (i) investigated the applicability of periodic redox processes of AC bioelectrodes for NB mineralization, focusing on carbon and nitrogen transformation and pollution control; (ii) elucidated electron transfer capabilities of AC bioelectrodes using electron balancing analysis, cyclic voltammetry, and electrochemical impedance spectroscopy; and (iii) revealed the growth characteristics, microbial community compositions, functional attributes, and metabolic pathways of biofilms on AC bioelectrodes using confocal laser scanning microscopy, metagenomics, metatranscriptomics, and non-targeted metabolomics. This AC bioelectrode offers a high-efficiency, low-carbon solution for the deep reduction of carbon and nitrogen pollution in RONC-laden wastewater.

Results and discussion

Performance of AC bioelectrodes in NB transformation

Stable removal of NB and total organic carbon (TOC) was maintained across five 120 h batch acclimation cycles, illustrating the effective initiation and sustained operation of all bioelectrodes under four electrical modes (Supplementary Fig. 1). The R^2 values for NB and TOC removal consistently exceeded 0.90 under the first-order kinetic model, whereas they fell below 0.90 under the second-order kinetic model (Supplementary Tables 1 and 2), indicating that the degradation of both NB and TOC adheres more closely to first-order kinetics. The NB removal followed first-order kinetics ($0.902 \le R^2 \le 0.993$), with kinetic constants (k) ranked as follows: sine-wave AC bioelectrode (0.054 ± 0.002) >square-wave AC bioelectrode (0.045 ± 0.001) > DC bioelectrode (0.041 ± 0.005) >open circuit (0.010 ± 0.001) (Fig. 1b and Supplementary Table 1). Notably, NB removal efficiencies with bioelectrodes were 1.77–1.83 times higher than those in the open circuit, highlighting the significant enhancement of microbial NB removal by electrical stimulation. Furthermore, sine- and square-wave AC bioelectrodes achieved NB removal rates of $97.58 \pm 0.09\%$ and $95.32 \pm 0.21\%$, respectively, surpassing the $94.21 \pm 1.58\%$ observed with DC bioelectrode. The higher efficacy of AC-driven periodic redox cycles over DC-driven reduction for NB removal further confirmed that alternating reduction and oxidation processes facilitated RONCs degradation[15]. This effect was likely due to the ability of oxidation processes to degrade reduction products of RONCs, thereby kinetically promoting further reduction of RONCs[3]. Additionally, during NB removal with AC bioelectrodes, sine-wave stimulation was more effective than square-wave stimulation. This improvement was attributed to the gradual voltage changes of sine waves, which are more readily adapted and utilized by electroactive microorganisms, thereby enhancing extracellular electron transfer (EET) between the microorganisms and the electrode, in contrast to the abrupt polarity reversals of square waves[16,17]. Sine-wave stimulation also showed greater potential to enhance microbial electroactivity, promote EET gene expression, and increase the production of redox-active mediators compared to square-wave stimulation[14].

As depicted in Fig. 1c, the ratio of intermediate product accumulation, represented by the accumulated AN to NB removal concentration, remained below 12% at 72 h for both sine- and square-wave AC bioelectrodes. These values were significantly lower than those observed in the DC bioelectrode (>50%) and open circuit (>40%). TOC removal followed a first-order kinetic model ($0.980 \le R^2 \le 0.994$), with k values ranked as: sine-wave AC bioelectrode (0.015 ± 0.027) >square-wave AC bioelectrode (0.012 ± 0.018) > DC bioelectrode (0.007 ± 0.019) >open circuit (0.002 ± 0.017) (Fig. 1d and Supplementary Table 1). TOC removal efficiency was substantially higher with sine- and square-wave AC bioelectrodes ($64.30 \pm 0.85\%$ and $57.51 \pm 0.57\%$) compared to the DC bioelectrode ($35.74 \pm 0.46\%$) and open circuit ($13.27 \pm 0.33\%$) (Fig. 1d). These results underscored that the redox processes occurring in AC bioelectrodes more effectively facilitated the further degradation and eventual mineralization of NB. Moreover, in AC bioelectrodes, sine-wave stimulation achieved higher intermediate product conversion than square-wave stimulation, effectively coupling the cathodic reduction of NB to AN with the anodic oxidation of AN to CO_2.

Following the reduction of NB to AN, the subsequent oxidative ring-opening of AN was accompanied by C − N bond cleavage, leading to the biotransformation of organic amines into inorganic nitrogen, primarily NH_4^+-N[3]. In sine- and square-wave AC bioelectrodes, NH_4^+-N concentrations after 72 h were 15.86 ± 2.12 mg/L and 21.90 ± 2.82 mg/L, respectively, lower than those in the DC bioelectrode (22.51 ± 0.70 mg/L) and open circuit (28.23 ± 2.80 mg/L) (Fig. 1e). Additionally, NO_3^--N concentrations followed the trend: sine-wave AC bioelectrode (2.01 ± 0.01 mg/L) <square-wave AC bioelectrode (2.93 ± 0.02 mg/L) <open circuit (2.95 ± 0.03 mg/L) < DC bioelectrode (4.55 ± 0.28 mg/L). The final concentrations of NH_4^+-N and NO_3^--N in the sine-wave AC were <20.0 mg/L and 2.5 mg/L, respectively, consistent with previous studies on the enhanced aniline degradation and simultaneous nitrogen removal by bioelectrochemical systems[18]. After 72 h, NO_2^--N concentrations in both sine-wave and square-wave AC were <0.1 mg/L, lower than those observed in DC (0.19 ± 0.01 mg/L) and open circuit (0.21 ± 0.02 mg/L) conditions (Fig. 1e). These results demonstrate that AC bioelectrodes exhibited the highest NH_4^+-N metabolism flux while maintaining the lowest residual concentrations of NO_3^--N and NO_2^--N, indicating that microorganisms in AC bioelectrodes effectively facilitated complete nitrification (NH_4^+ to NO_3^-) and denitrification (NO_3^- to N_2) processes. Meanwhile, the residual total nitrogen (TN) followed the trend: sine-wave AC bioelectrode (25.61 ± 1.14 mg/L) <square-wave AC bioelectrode (35.50 ± 3.54 mg/L) < DC bioelectrode (51.52 ± 3.56 mg/L) <open circuit (82.49 ± 3.48 mg/L). Compared to DC bioelectrode and open circuit, AC bioelectrodes exhibited the highest efficiency in NB reduction and AN oxidation (Fig. 1b-d). These results indicate that AC bioelectrodes efficiently achieved deep mineralization of NB while also enhancing nitrogen removal, thus reducing

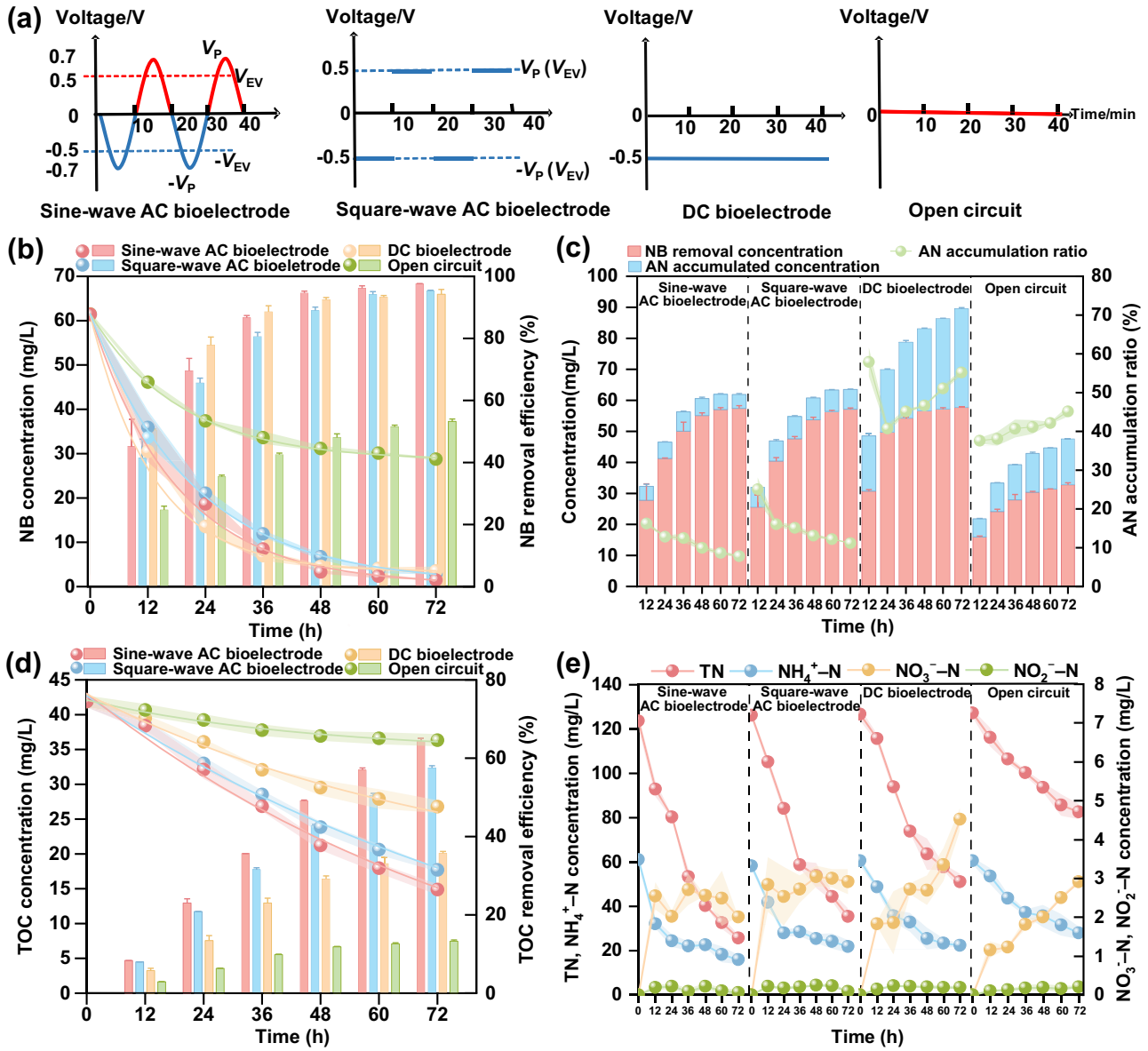

Fig. 1 | Performance of NB transformation under sine-wave AC, square-wave AC, DC, and open-circuit bioelectrodes. a Voltage waveforms (V_P: peak voltage; V_{EV}: effective voltage); (**b**) Time-course changes in NB concentration and removal efficiencies; (**c**) Accumulated AN concentration, NB removal concentration, and AN accumulation ratio; (**d**) Time-course changes in TOC concentration and removal efficiencies; (**e**) Time-course changes in TN, NH_4^+, NO_3^-, and NO_2^- concentrations.

the nitrogen load in subsequent treatment stages. In AC bioelectrodes, sine-wave stimulation achieved higher removal rates of NH_4^+-N, NO_3^--N, and TN compared to square-wave, likely due to the enhanced activity of nitrifying and denitrifying bacteria stimulated by the continuous gradient of electrical stimulation[19]. Electro-hydrodynamic forces induced by the continuous gradient of electrical stimulation enhance plasma membrane permeability, promoting efficient nutrient and material transfer across the cell membrane[12,19]. This process significantly augments microbial metabolic activity and boosts electron transfer capacity.

While AC stimulation has demonstrated potential in enhancing nitrification and denitrification, microbial responses are highly dependent on wastewater composition and environmental conditions. Factors such as pH, temperature, and nutrient availability significantly influence the performance of bioelectrodes in real wastewater. Deviations from the optimal pH can inactivate key enzymes and diminish electrochemical activity, reducing pollutant removal efficiency[20]. Similarly, temperatures outside the microorganisms' tolerance range suppress metabolic activity, impairing current output and pollutant degradation efficiency[21]. Adequate nutrient availability accelerates biofilm formation, fostering the development of an optimally thick biofilm on the electrode surface, which enhances conductivity[22]. Addressing these environmental variables, particularly through pilot-scale studies, is crucial for optimizing bioelectrode performance under the diverse conditions encountered in WWTPs. Future applications could employ an adaptive electrochemical control strategy, utilizing real-time monitoring of parameters alongside data-driven control models to dynamically adjust to environmental fluctuations, enhancing technology scalability and applicability.

Electrochemical and growth characteristics of electroactive biofilms

In both sine- and square-wave AC bioelectrodes, the current direction exhibited periodic alternations, indicating stable transitions between reduction (negative current) and oxidation (positive current) processes (Fig. 2a, b). The current in the DC bioelectrode exhibited a fluctuating curve before stabilizing at −0.25 mA (Supplementary Fig. 2), which was significantly lower than the effective current values observed in the AC

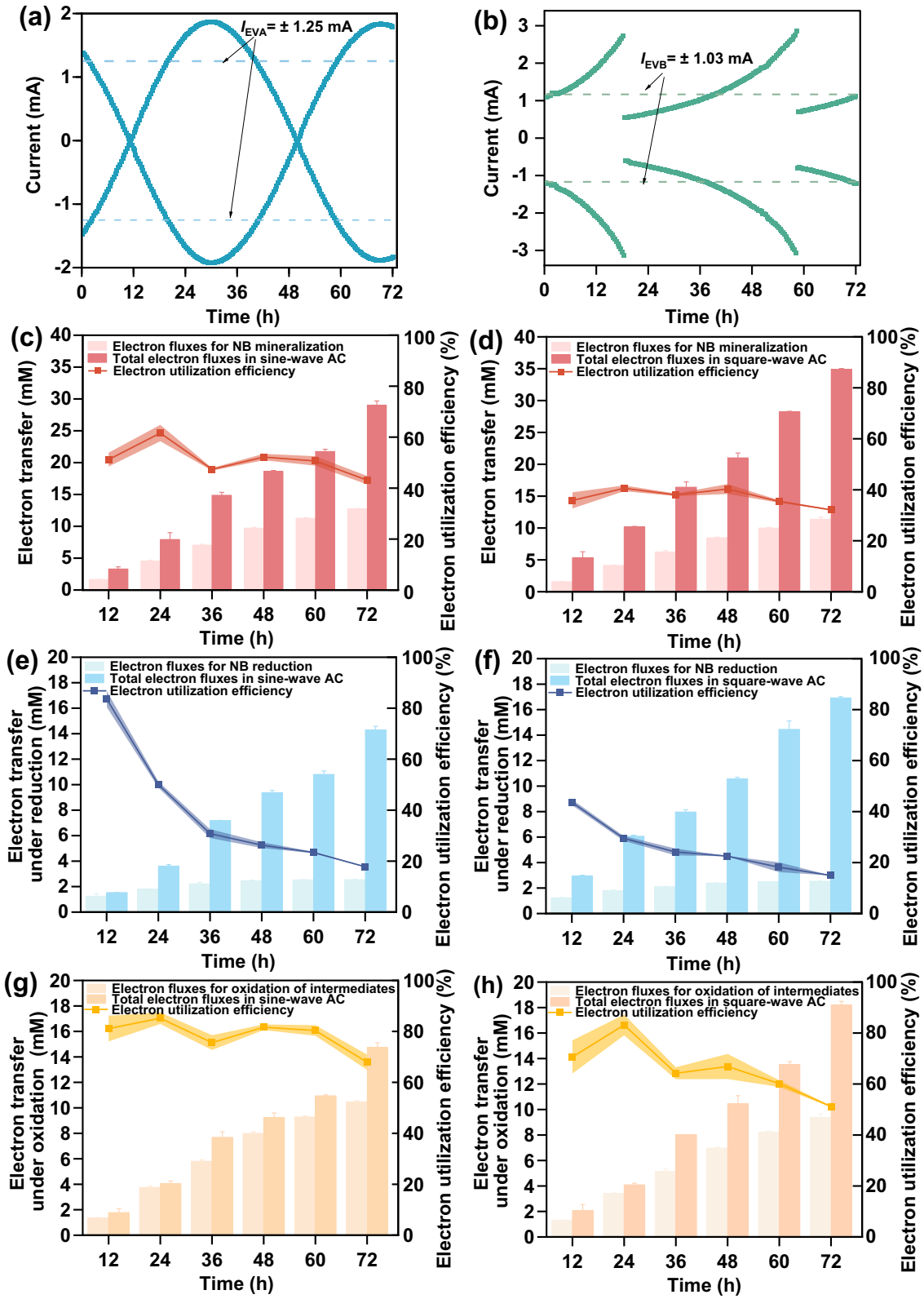

Fig. 2 | Current variation and electron utilization efficiency under sine-wave AC and square-wave AC bioelectrodes. a Current responses under sine-wave AC with corresponding effective values (I_{EVA} and I_{EVB}); (**b**) Current responses under square-wave AC with corresponding effective values (I_{EVA} and I_{EVB}); (**c**, **e**) and (**g**) Electron utilization performance during the entire reaction period, reduction period, and oxidation period for sine-wave AC; (**d**, **f**) and (**h**) Electron utilization performance during the entire reaction period, reduction period, and oxidation period square-wave AC.

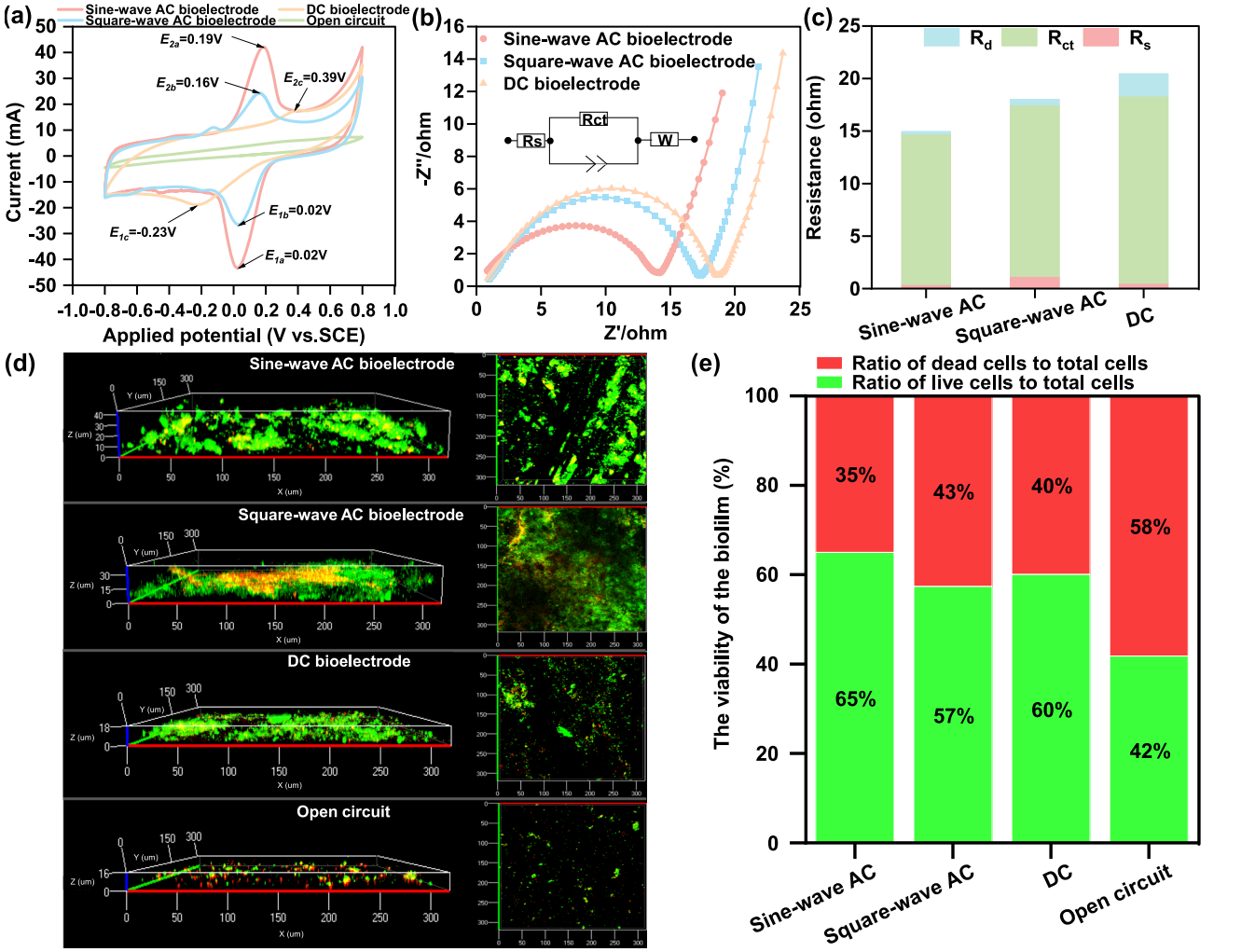

Fig. 3 | Electrochemical activity and biofilm colonization characteristics of sine-wave AC, square-wave AC, DC, and open-circuit bioelectrodes. a Cyclic voltammetry (CV) profiles; (**b**) Nyquist plots obtained from electrochemical impedance spectroscopy (EIS), with an inset showing the equivalent circuit model for different electrical modes (Z' and Z" represent the real and imaginary parts of the complex impedance, respectively; W denotes the Warburg element, and CPE the constant phase element); (**c**) Total internal resistances from equivalent circuit fitting, including R_s (ohmic resistance), R_{ct} (charge transfer resistance), and R_d (finite diffusion resistance); (**d**) 3D and 2D structural images of electrode biofilms; (**e**) Ratio of live to dead cells based on pixel counting.

bioelectrodes. In AC bioelectrodes, effective current value of the sine-wave (I_{EVA} = ± 1.25 mA) was 1.21 times greater than that of the square-wave (I_{EVB} = ± 1.03 mA). The square-wave AC bioelectrode, characterized by instantaneous electrode polarity reversals, could lead to higher ohmic losses and negatively impact ion transmission[16], potentially reducing current amplitude. Generally, the higher current observed in sine-wave AC bioelectrode could promote the growth of electroactive biofilms and enhance their catalytic activity[23]. Throughout the reaction period, the electron utilization efficiency (EUE) in sine-wave AC bioelectrode reached 43.09 ± 1.67%, 1.38 times higher than in square-wave AC (32.12 ± 0.23%) at 72 h (Fig. 2c, d). This suggested that electroactive biofilms in sine-wave AC bioelectrode possessed enhanced electron utilization capabilities for NB degradation[24]. During the reduction phase (Fig. 2e, f), the average EUE for sine-wave AC was 18.72 ± 0.10%, higher than for square-wave AC (16.93 ± 0.10%). Although total electron fluxes in sine-wave AC were lower than those in square-wave AC, the electron fluxes utilized for NB reduction in both modes were almost identical (2.55 mM/L vs. 2.53 mM/L), indicating that sine-wave AC-stimulated biofilm more efficiently channeled electrons toward NB reduction. During the oxidation phase (Fig. 2g, h), the EUE of sine-wave AC (67.91 ± 2.90%) markedly exceeded that of square-wave AC (51.18 ± 0.28%). Despite lower total electron fluxes in sine-wave AC compared to square-wave AC, the electron fluxes available for AN oxidation were nearly the same in both modes (10.48 mM/L vs. 9.37 mM/L), suggesting that sine-wave AC-stimulated biofilm more effectively harvested electrons from intermediates oxidation. In the redox phase, sine-wave AC stimulation demonstrated a higher EUE, indicating that its electroactive biofilm possessed a strong ability for electron release and storage. This capability reflects the pseudocapacitive characteristics of the biofilm, representing the dynamic-controlled electron transfer process[25]. Therefore, sine-wave AC-stimulated biofilms exhibited enhanced electron transfer capabilities, leading to more efficient NB reduction and intermediate oxidation.

The area enclosed by the cyclic voltammetry (CV) curves varied significantly across different bioelectrodes (Fig. 3a), with the following ranking: sine-wave AC bioelectrode (45.63) >square-wave AC bioelectrode (35.54) > DC bioelectrode (27.04) >open circuit (4.75). This trend aligned with the observed NB degradation activity (Fig. 1). The CV curves of AC and DC bioelectrodes, excluding the open circuit, exhibited distinct reduction and oxidation peaks with notable asymmetry, indicating the irreversible nature of primary NB degradation at the bioelectrode interface. The reduction peak of the DC bioelectrode appeared at –0.23 V, corresponding to the reduction of the nitro group in NB[26]. The reduction peaks of sine- and square-wave AC bioelectrodes showed positive shifts of 0.25 V compared to the DC bioelectrode, with peak currents ranked as follows: sine-wave AC

(43.28 mA) >square-wave AC (26.44 mA) > DC (18.93 mA). Additionally, distinct oxidation peaks at 0.16 V were observed in both sine- and square-wave AC bioelectrodes, while a weaker peak at 0.39 V was seen in the DC bioelectrode. These oxidation peaks, attributed to AN oxidation[27], had a peak current 1.73 times higher in sine-wave AC compared to square-wave AC. The lower potential threshold for triggering reduction and oxidation reactions, along with the significant increase in reaction current, indicated that the sine-wave AC bioelectrode effectively enhanced microbial electrocatalytic activity for NB degradation.

The electrochemical impedance spectroscopy (EIS) spectra were analyzed using an equivalent circuit model including the ohmic resistance (R_s), the charge transfer resistance (R_{ct}), and the finite diffusion resistance (R_d) (Fig. 3b)[28]. The analysis showed that R_s for sine-wave AC bioelectrodes was 0.39 Ω, lower than that for square-wave AC and DC bioelectrodes (Fig. 3c). This lower R_s indicated superior electron conductivity in sine-wave AC-stimulated biofilms[29], which corresponded with enhanced NB degradation and higher current generation. R_{ct}, the dominant resistance component, was ranked as follows: sine-wave AC (14.35 Ω) <square-wave AC (16.35 Ω) <DC (17.81 Ω). The lower R_{ct} for sine-wave AC biofilms reflects improved pseudocapacitive behavior and increased substrate degradation efficiency[30]. Additionally, the R_d for sine-wave AC was 0.23 Ω, lower than square-wave AC (0.53 Ω) and DC bioelectrodes (2.12 Ω), indicating enhanced diffusion across the biofilm and bioelectrode[29]. Notably, the impedance results from EIS showed an inverse correlation with the current density produced by the bioelectrodes. As shown in Supplementary Fig. 3, the current density in the DC bioelectrode eventually stabilized at −9.50 mA/cm^2, lower than that in the sine-wave AC (39.80 mA/cm^2) and square-wave AC (32.80 mA/cm^2) bioelectrodes. Thus, the sine-wave AC bioelectrode, with its minimum impedance and maximum current density, demonstrated optimal performance in NB degradation (Fig. 1). However, the ideal conditions for minimizing polarization effects in sine-wave AC bioelectrodes require further investigation, particularly regarding the regulation of frequency and amplitude.

Scanning electron microscope (SEM) images of the biofilms provided preliminary insights into microbial density and adherence. The sine-wave AC bioelectrode exhibited optimal microbial enrichment, followed by the square-wave AC bioelectrode, the DC bioelectrode, and finally the open circuit (Supplementary Fig. 4). Further, confocal laser scanning microscope (CLSM) images revealed differences in biofilm thickness and the distribution of live and dead bacteria under various electrical stimulations. Biofilm thickness was ranked as follows: sine-wave AC bioelectrode (40 μm) >square-wave AC bioelectrode (35 μm) >DC bioelectrode (18 μm) >open circuit (16 μm) (Fig. 3d). The increased biomass in AC bioelectrodes, particularly under sine-wave stimulation, likely results from enhanced microbial EET and substrate metabolism[31]. Increased biofilm thickness would improve the functionality and stability of the electrode interface's microecosystem, enhancing resilience against physical and chemical stresses, nutrient scarcity, and external toxins[28]. Furthermore, the electromicrobiome's vitality was notably influenced by the type of current applied, with sine-wave AC showing the highest activity, reflected in a 65% live cell ratio at the sine-wave AC bioelectrode. This outperformed the DC bioelectrode (60%) and the open circuit (42%) (Fig. 3e). Under square-wave stimulation, a distinct layer of dead cells was observed in the biofilm, likely resulting from the cumulative damage caused by abrupt polarity reversals within the microcolony[19]. This necrotic layer disrupts the secretion of electroactive mediators, impairs interspecies electron transfer, and reduces biofilm conductivity, collectively diminishing the biofilm's electroactivity[28]. EIS results revealed a close correlation between reduced biofilm electroactivity and an increased R_{ct}. In contrast, sine-wave stimulation did not induce a comparable dead-cell layer, suggesting improved biofilm growth and renewal dynamics. These favorable conditions enhanced biofilm electrochemical performance, facilitating more efficient NB degradation.

Microbial community composition and function

Alpha diversity indices, including Shannon, Shannoneven, Simpsoneven, and Pielou_e, indicated that the sine-wave AC bioelectrode had the most diverse microbial composition, which was beneficial for executing the complex redox processes involved in NB degradation (Supplementary Table 3). Beta diversity analysis further revealed significant differences in the microbial community structure across bioelectrodes under different electrical stimulations (Supplementary Fig. 5a, b). Non-metric multidimensional scaling (NMDS) analysis showed clear separation along the NMDS1 axis between bio-samples with electrical stimulation (closed circuit) and without stimulation (open circuit), while different types of electrical stimulation (sine-wave AC, square-wave AC, and DC) led to distinct separation along the NMDS2 axis. The microbial community composition at the phylum and class levels (Supplementary Fig. 6a, b) was shown in the Supplementary Note 1 and further confirmed that electrical stimulation condition significantly influences the structure of bioelectrode biofilms.

At the genus level, electrical stimulation and NB selection significantly enriched functional microbial communities within the electrode biofilms, including nitro-reducing, aromatic-oxidizing, ammonia-oxidizing, denitrifying bacteria, and electrochemically active bacteria (EAB), with notable variations in abundance across different electrical modes (Fig. 4a). *Desulfovibrio*, crucial for NB removal via sequential reduction of nitro group to nitroso, hydroxylamino, and amino groups under anaerobic conditions[32], was most abundant under sine-wave AC (1.20%), being 2–4 time as prevalent as under square-wave AC (0.60%), DC (0.50%) and open circuit (0.30%). *Sphingopyxis*, known for oxidizing aromatic amines through hydroxylation, ring cleavage, and secondary metabolite degradation[15], dominated across all modes, with the highest abundance under sine-wave AC (8.50%) followed by square-wave AC (8.40%), DC (1.70%), and open circuit (0.30%). *_f_Chitinophagaceae*, an ammonia-oxidizing bacterium converting NH_4^+ to NO_3^-[33], was most abundant under sine-wave AC (2.00%). *_p_Bacteroidota*, involved in denitrification using electrons from cytochrome c during polarity reversals[34], had abundances of sine-wave AC (1.80%) >square-wave AC (1.32%) >DC (1.30%) >open circuit (1.10%). Notably, *Geobacter*, recognized for its bidirectional EET capabilities and effective pollutant transformation[35], exhibited abundances of sine-wave AC (5.20%) >square-wave AC (2.50%) >DC (0.30%) >open circuit (0.07%).

Predominant genera in electrode biofilms were categorized into five functional clusters: nitro-reduction, aromatic-oxidation, ammonia-oxidation, denitrification, and electron transfer (Fig. 4b). Under sine-wave AC, nitro-reducing bacteria, including *Clostridium*[32], *Geobacter*, and *Desulfovibrio*[35], were significantly more abundant at 6.90% compared to 3.40% under square-wave AC, 1.00% under DC, and 0.75% under open circuit. Sine-wave AC also enhanced the abundance of aromatic-oxidizing bacteria such as *Sphingopyxis* and *Acidovorax*[36,37], with 9.30% compared to 9.00% under square-wave AC, 1.90% under DC, and 0.50% under open circuit. Ammonia-oxidizing bacteria, including *_f_Chitinophagaceae* and *Aquamicrobium*[33,38], were most prevalent under sine-wave AC (6.30%), followed by square-wave AC (5.50%), DC (2.30%), and open circuit (1.50%). Denitrifying bacteria, such as *_p_Bacteroidota* and *_o_Bacteroidales*[39], were also most abundant under sine-wave AC (5.80%), compared to 5.10% under DC, 4.70% under square-wave AC, and 4.00% under open circuit. EAB, including *Geobacter*[35], *Sphaerochaeta*[40], and *Desulfovibrio*[35], were also most enriched under sine-wave AC (7.60%), compared to square-wave AC (3.56%), DC (1.10%), and open circuit (1.07%). The abundance of nitro-reducing, aromatic-oxidizing bacteria, and EAB was significantly correlated with NB reduction, intermediate oxidation, and electron utilization efficiency, respectively. This suggested that the efficient enrichment of functional bacterial communities under sine-wave AC stimulation supported the high-efficiency mineralization of NB.

Key functional genes and metabolic pathways

Metagenomic sequencing revealed significant changes in key functional genes involved in redox processes and electron transfer during NB degradation across the four electrode modes (Fig. 4c, d). Under sine-wave AC

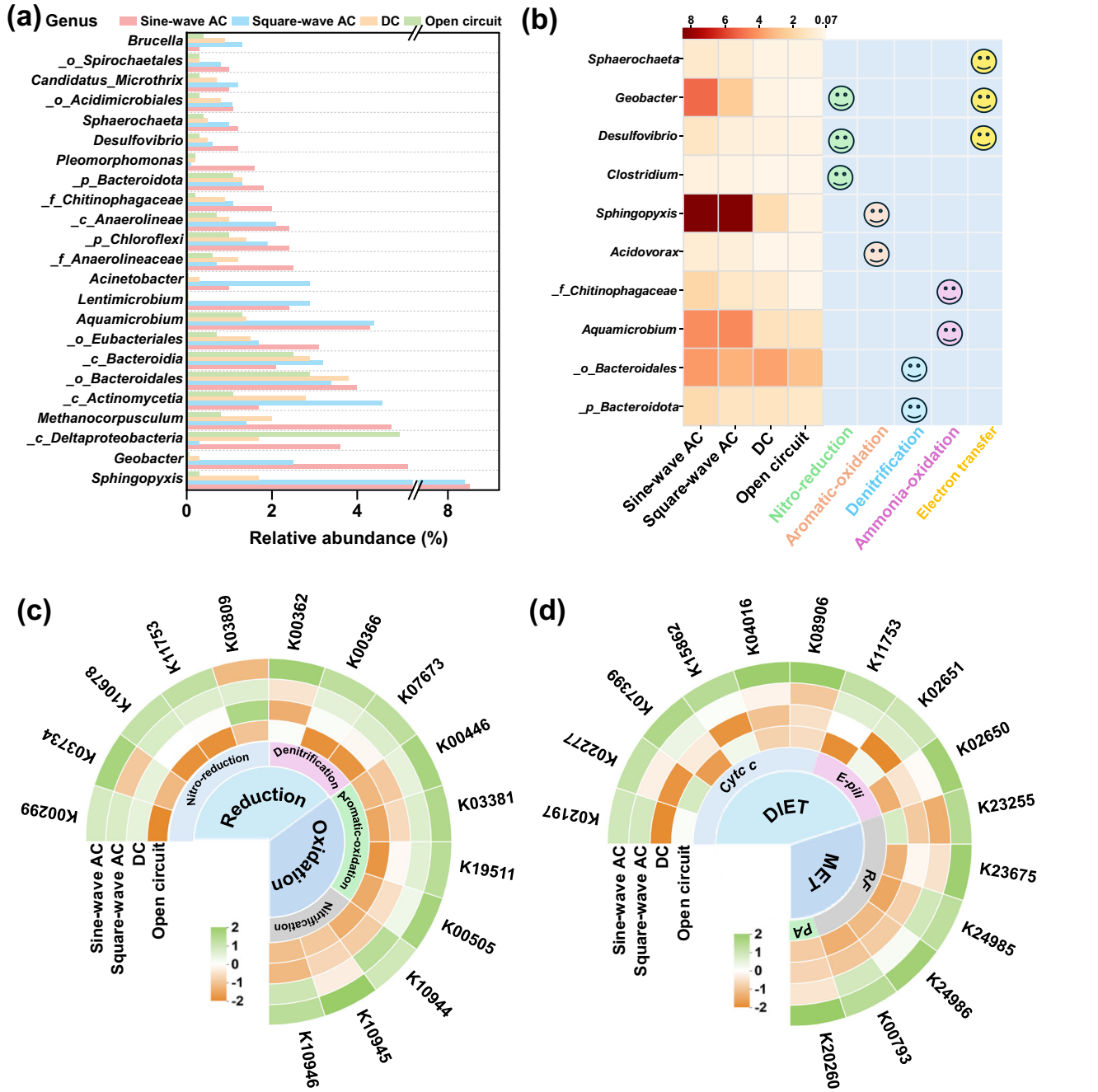

Fig. 4 | Key bacterial genera and functional gene composition of electrode biofilms under sine-wave AC, square-wave AC, DC, and open-circuit conditions. **a** Dominant bacterial genera; (**b**) Specific functional genera categorized as nitro-reducing bacteria, aromatic-oxidizing bacteria, ammonia-oxidizing bacteria, denitrifying bacteria, and electroactive bacteria; (**c**) Genes associated with nitro-reduction, nitrate- and nitrite-reduction (denitrification), aromatic-oxidation, and ammonia-oxidation (nitrification); (**d**) Genes involved in the biosynthesis of cytochromes c (Cytc c), riboflavin (RF), phenazine (PA), and E-pili under different electrical modes (DIET: direct interspecies electron transfer; MET: mediated electron transfer).

stimulation, nitroreductase (K10678) and NAD(P)H dehydrogenase (K03809) were most abundant, reflecting enhanced NB reduction to AN via the NAD(P)H chain[41]. Catechol dioxygenase, crucial for aromatic ring cleavage[27], likely facilitated the mineralization of NB intermediates (e.g., AN). Ammonia oxidation to nitrate involved ammonia monooxygenase[42], while denitrification required nitrate and nitrite reductases[39]. Notably, under sine-wave AC, the TPM of catechol dioxygenase (K00446 and K03381), nitrate and nitrite reductases (K00362, K00366, and K07673), and ammonia monooxygenase (K10944, K10945, and K10946) was significantly higher compared to other bioelectrodes. This trend was consistent with the higher abundance of associated host bacteria (Fig. 4c), including *Desulfovibrio* for nitroreductase[43], *Sphingopyxis* for catechol dioxygenase[14], *_o_Bacteroidales* and *_p_Bacteroidota* for nitrate and nitrite reductase[44], and *_f_Chitinophagaceae* for ammonia monooxygenase[45].

During electrode-dependent NB degradation, direct EET occurred via interactions between electrodes and microbes through c-type cytochromes and e-pili, while indirect EET was mediated by redox mediators like riboflavin and phenazine. Compared to open circuit and DC bioelectrodes, AC bioelectrodes, particularly under sine-wave conditions, significantly enriched EET-related genes. These included genes for cytochromes (K02197, K02277, K07399, K15862, K04016, and K08906), e-pili (K02651, K02650, and K23255), riboflavin (K11753, K23675, K24985, K24986, and K00793), and phenazine (K20260) (Fig. 4d)[46]. Simultaneously, functional bacterial genera such as *Geobacter*, *Desulfovibrio*, and *Sphaerochaeta*, which harbor

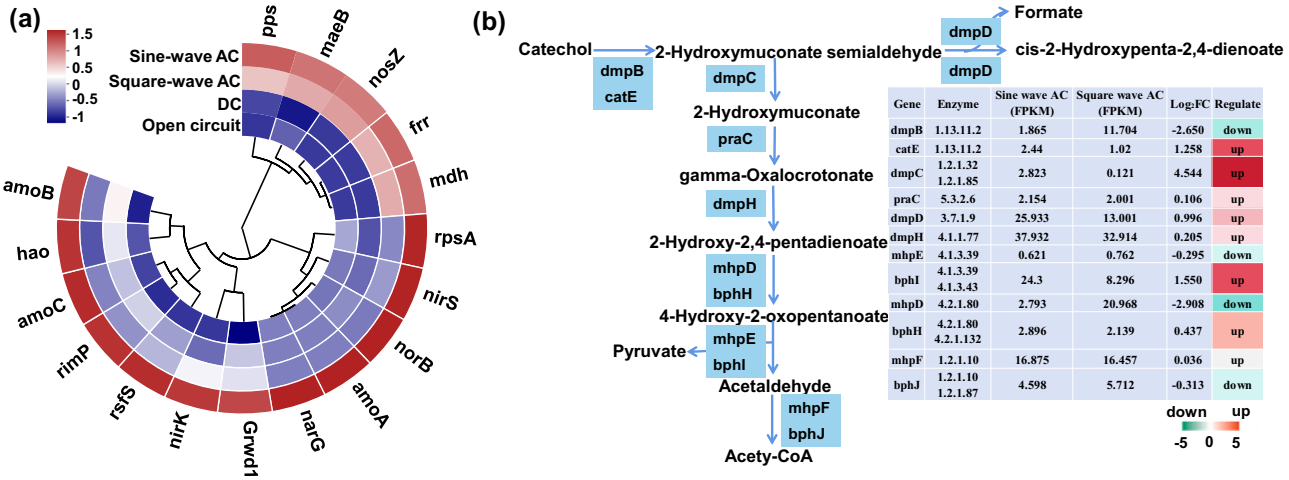

Gene	Enzyme	Sine wave AC (FPKM)	Square wave AC (FPKM)	Log_2FC	Regulate
dmpB	1.13.11.2	1.865	11.704	-2.650	down
catE	1.13.11.2	2.44	1.02	1.258	up
dmpC	1.2.1.32 1.2.1.85	2.823	0.121	4.544	up
praC	5.3.2.6	2.154	2.001	0.106	up
dmpD	3.7.1.9	25.933	13.001	0.996	up
dmpH	4.1.1.77	37.932	32.914	0.205	up
mhpE	4.1.3.39	0.621	0.762	-0.295	down
bphI	4.1.3.39 4.1.3.43	24.3	8.296	1.550	up
mhpD	4.2.1.80	2.793	20.968	-2.908	down
bphH	4.2.1.80 4.2.1.132	2.896	2.139	0.437	up
mhpF	1.2.1.10	16.875	16.457	0.036	up
bphJ	1.2.1.10 1.2.1.87	4.598	5.712	-0.313	down

Fig. 5 | Genes involved in carbon and nitrogen transformations. a Metatranscriptomics analysis of genes involved in ribosome, carbon metabolism, and nitrogen metabolism pathways under sine-wave AC, square-wave AC, DC and open-circuit bioelectrodes; (**b**) The catechol meta-cleavage pathway and expression of key genes under sine-wave and square-wave AC bioelectrodes.

these genes, also showed similar enrichment patterns (Fig. 4b). From a KEGG pathway perspective, AC stimulation notably enhanced metabolic functions related to carbohydrate metabolism, amino acid metabolism, transport and catabolism, and cellular communities in prokaryotes (Supplementary Fig. 7), highlighting the enhanced electroactive behavior of bioelectrodes for NB degradation under sine-wave AC conditions (details in Supplementary Note 2).

Metatranscriptomics analysis of carbon and nitrogen transformations

Transcriptomic analysis revealed distinct metabolic pathways across different electrical stimulation modes (Supplementary Fig. 8), highlighting the advantages of AC-driven bioelectrodes in NB mineralization. Principal coordinates analysis (PCoA) indicated significant mode-specific differences, with PC1 and PC2 explaining 60.39% and 22.79% of the variance, respectively (Supplementary Fig. 9). Sine-wave AC bioelectrode showed a notably higher ratio of upregulated to down-regulated genes (Supplementary Fig. 10), indicating enhanced metabolic activity during NB degradation. KEGG pathway analysis identified key up-regulations in pathways associated with ribosomes, aromatic compound degradation, carbon metabolism, and nitrogen metabolism under AC stimulation (Supplementary Fig. 8). Genes involved in ribosome synthesis (e.g., *rpsA*, *rimP*, *frr*, *Grwd1*, and *rsfS*) were significantly upregulated (Fig. 5a), promoting intracellular processes crucial for growth, energy production, and metabolism, which supported enhanced NB mineralization and nitrogen removal[47]. The meta-cleavage of catechol, a critical step in aromatic oxidation driven by bacteria like *Sphingopyxis*[3], exhibited the highest activity under sine-wave AC. Elevated expression of aromatic oxidation genes (*dmpC, dmpD, dmpH*, *catE*, *praC*, *bphI, bphH*, and *mhpF*) under sine-wave AC resulted in increased biocatalytic activity and accelerated cleavage of intermediates (Fig. 5b). In nitrogen metabolism, genes encoding nitrate and nitrite reductases (*nosZ*, *norB*, *nirS*, *nirK*, and *narG*) and nitrification-related genes (*narG*, *Hao*, *amoA*, *amoB*, and *amoC*) were most abundant under sine-wave AC, demonstrating significant enhancements in both nitrification and denitrification processes. Notably, key metabolites from catechol degradation, such as pyruvate and acetyl-CoA, entered the carbon metabolism pathway, where NADPH and ATP supported nitro-reduction, denitrification, and cell viability under anaerobic conditions[19]. The internal generation of small organic molecules from catechol degradation met the metabolic demands for nitro-reduction and denitrification, eliminating the need for external carbon sources in AC-stimulated bioelectrodes. Genes involved in carbon metabolism (*mdh, pps, maeB*) were highly expressed under sine-wave AC (Fig. 5a), correlating with superior performance in nitro-reduction, TOC, and TN removal. This comprehensive genomic response underscores the enhanced functionality of microbial communities in sine-wave AC-stimulated biofilms for optimal NB mineralization.

Non-targeted metabolomics identification and toxicity assessment of active metabolites

Metabolomic profiling under different electrical stimulations was analyzed using Venn diagrams to distinguish common and unique metabolic products (Fig. 6a). The comparison between sine-wave and square-wave conditions revealed only 14 differential metabolites, suggesting a substantial overlap in metabolic pathways under AC bioelectrodes. Furthermore, co-metabolic testing identified specific metabolic products across different electrical stimulations (Fig. 6b). Metabolite concentrations were visually represented with a color gradient from blue (low concentration) to red (high concentration) for ease of interpretation. Key intermediates, such as nitrosobenzene and AN, crucial in the reduction process of NB, were identified[48]. Additional significant intermediates, such as phenol and p-hydroxybenzoic acid, were detected during the process, serving as key precursors to ring-opening oxidation[3,18]. Final small molecular acids, such as pyruvate, succinic acid, and salicylic acid, resulting from the oxidative ring opening of AN, were observed, consistent with previous findings[49]. KEGG pathway annotations further identified trans-cinnamic acid and caffeic acid as small molecular products following AN ring-opening metabolism. These metabolites were highlighted in red squares, indicating their elevated production under sine-wave AC stimulation. This finding emphasized the impact of electrical stimulation modes on specific metabolic pathways, demonstrating sine-wave AC's enhanced efficacy in promoting biochemical reactions favorable to NB biomineralization.

To evaluate the toxicity of key intermediates prior to mineralization, the Toxicity Estimation Software Tool (T.E.S.T.) was employed to estimate bioconcentration factors and acute toxicity. The bioconcentration factor indicates a substance's bioaccumulation potential in aquatic organisms, while acute toxicity reflects its harmful effects on aquatic life[50]. Compared to NB, AN exhibited lower bioconcentration factors and acute toxicity grades (Supplementary Fig. 11), suggesting that the reduction of NB to AN significantly mitigates environmental risks associated with water contamination. AN was further oxidized to catechol or p-hydroxybenzoic acid and ultimately mineralized into non-toxic small organic acids, such as pyruvate, thereby further reducing water toxicity. Notably, sine-wave AC bioelectrodes achieved 90.9% mineralization of intermediates, leaving only a minimal fraction of residual byproducts. However, the potential

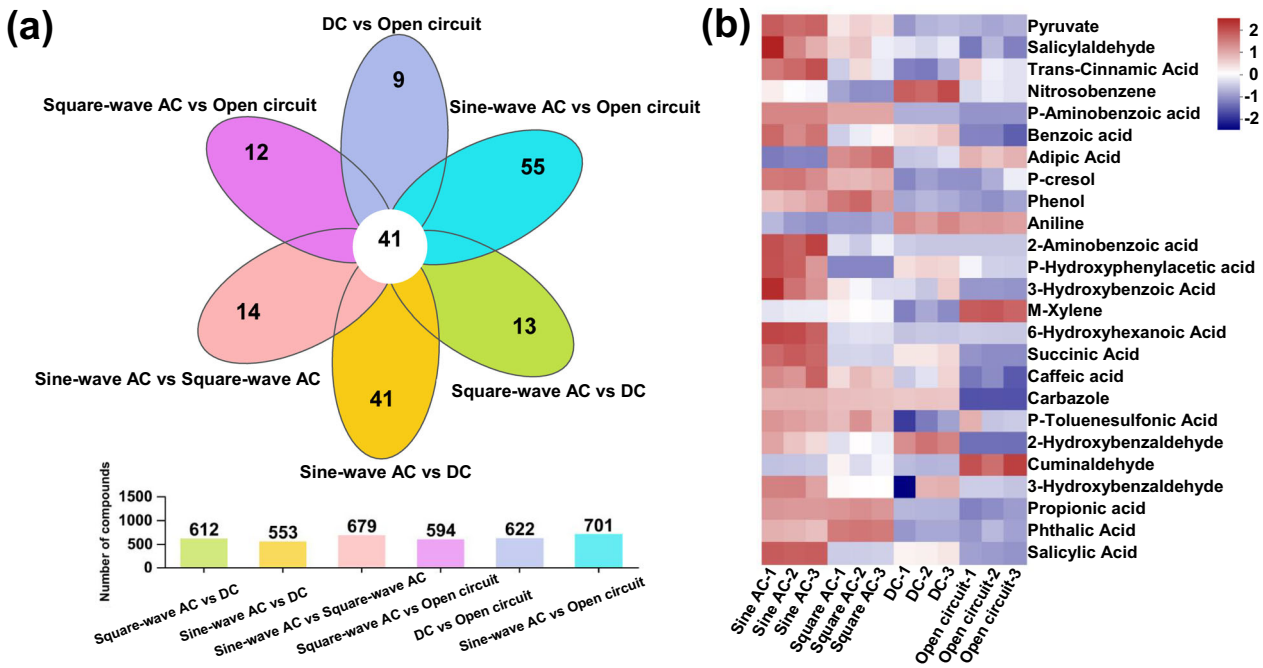

Fig. 6 | Non-targeted metabolomics identification of active metabolites under sine-wave AC, square-wave AC, DC, and open-circuit bioelectrodes. a Venn diagram showing common and unique metabolites; (**b**) Heatmap of metabolite profiles.

environmental risks of these residual intermediates in practical applications warrant further attention. Comprehensive and precise toxicity assessments, along with continued optimization of bioelectrode performance, are essential to ensure the safety and effectiveness of these systems in real-world wastewater treatment scenarios.

A mechanistic model for AC-driven redox in efficient mineralization of RONCs

Leveraging insights into NB mineralization efficiency, degradation pathways, electromicrobiome dynamics, and gas chromatography-mass spectrometry (GC-MS) spectra integrated with non-targeted metabolomics (Supplementary Fig. 12 and Fig. 6b), a detailed mechanism and potential metabolic pathways for AC-driven bioelectrodes in NB mineralization were proposed (Fig. 7a, b). The AC-stimulated NB degradation cycle involves alternating reduction and oxidation stages that enhance RONC breakdown. During the reduction phase, sine-wave AC stimulation demonstrated superior effectiveness compared to other modes, achieving NB removal rates ~1.09–1.15 times higher. Sine-wave AC stimulation selectively enriched nitro-reducing bacteria in the biofilm, increasing their abundance by 1.25–2.14 times relative to other modes. Electrons from the bioelectrode drive the reduction of NB to AN, a process primarily regulated by *Desulfovibrio* and nitroreductase (encoded by *nbzA*) (Fig. 7b). In the oxidation phase, AN, a primary intermediate in NB reduction, undergoes further degradation. Sine-wave AC stimulation significantly enhanced AN removal efficiency, surpassing other modes by 1.25–4.17 times based on the ratios of accumulated intermediate products. Sine-wave AC-stimulated biofilms exhibited substantial enrichment of aromatic-oxidizing bacteria and associated catechol dioxygenase genes, facilitating AN mineralization. Under sine-wave AC stimulation, AN was oxidized to phenol or 2,6-dihydroxybenzoic acid, which were subsequently converted to catechol and resorcinol, respectively. These compounds were further oxidized to smaller organic acids, such as pyruvic and succinic acid, under the regulation of *Sphingopyxis* and catechol oxygenase (encoded by *dmpB/C/catE* and *tsdB/chqB*) (Fig. 7b). EAB such as *Geobacter*, known for their bidirectional electron transfer capabilities, were also selectively increased by 2.15–4.09 times compared to other modes. The sine-wave AC-stimulated biofilm showed a higher presence of genes associated with EAB, including those involved in cytochrome, phenazine, riboflavin, and e-pili biosynthesis.

Furthermore, the redox process facilitated not only the degradation of organic nitrogen compounds but also the transformation of inorganic nitrogenous compounds. NH_4^+, released during AN degradation, was oxidized to NO_3^- under the regulation of *Aquamicrobium* and ammonia oxidase (encoded by *AmoA/B/C*). Subsequently, NO_3^- was reduced to N_2 during denitrification, driven by_*o_Bacteroidales* and regulated by genes such as *napA/B/nirK/S/norB/C/nosZ*, which encode nitrate/nitrite reductases (Fig. 7b). Sine-wave AC stimulation was particularly effective in this context, as evidenced by the increased presence of genes related to ammonia oxidase and nitrate/nitrite reductases. This mode promoted the enrichment of critical pathways for RONCs and nitrogen metabolism, aligning with enhanced activity in ribosome and carbon metabolism pathways, which are pivotal for energy transfer and electron transport during redox reactions. Genes involved in key metabolic pathways and active metabolites were upregulated under sine-wave AC stimulation, highlighting the synergistic effects of multi-pathway interactions.

The reactor configuration and operational parameters, such as amplitude and frequency, are pivotal in optimizing conditions that balance microbial activity while minimizing polarization effects, thereby significantly enhancing the efficacy of NB removal[19]. Further refinement of these parameters is essential for improving NB elimination performance and represents a critical focus for future research. Meanwhile, the application of bioelectrodes in full-scale WWTPs may be influenced by various factors, including wastewater flow rate, composition, pH, microbial community dynamics, and electrode spacing, all of which impact treatment efficiency[51]. Scaling up the application of bioelectrodes in wastewater treatment also faces challenges such as low treatment efficiency, limited energy output, high capital costs, and elevated internal resistance[52]. To overcome these barriers, future research should prioritize transitioning from laboratory-scale studies to pilot- and commercial-scale applications, with an emphasis on optimizing AC bioelectrode configurations. Moreover, comprehensive system evaluations, including cost-effectiveness and energy efficiency analyses, will be essential for determining their viability in real-world WWTPs.

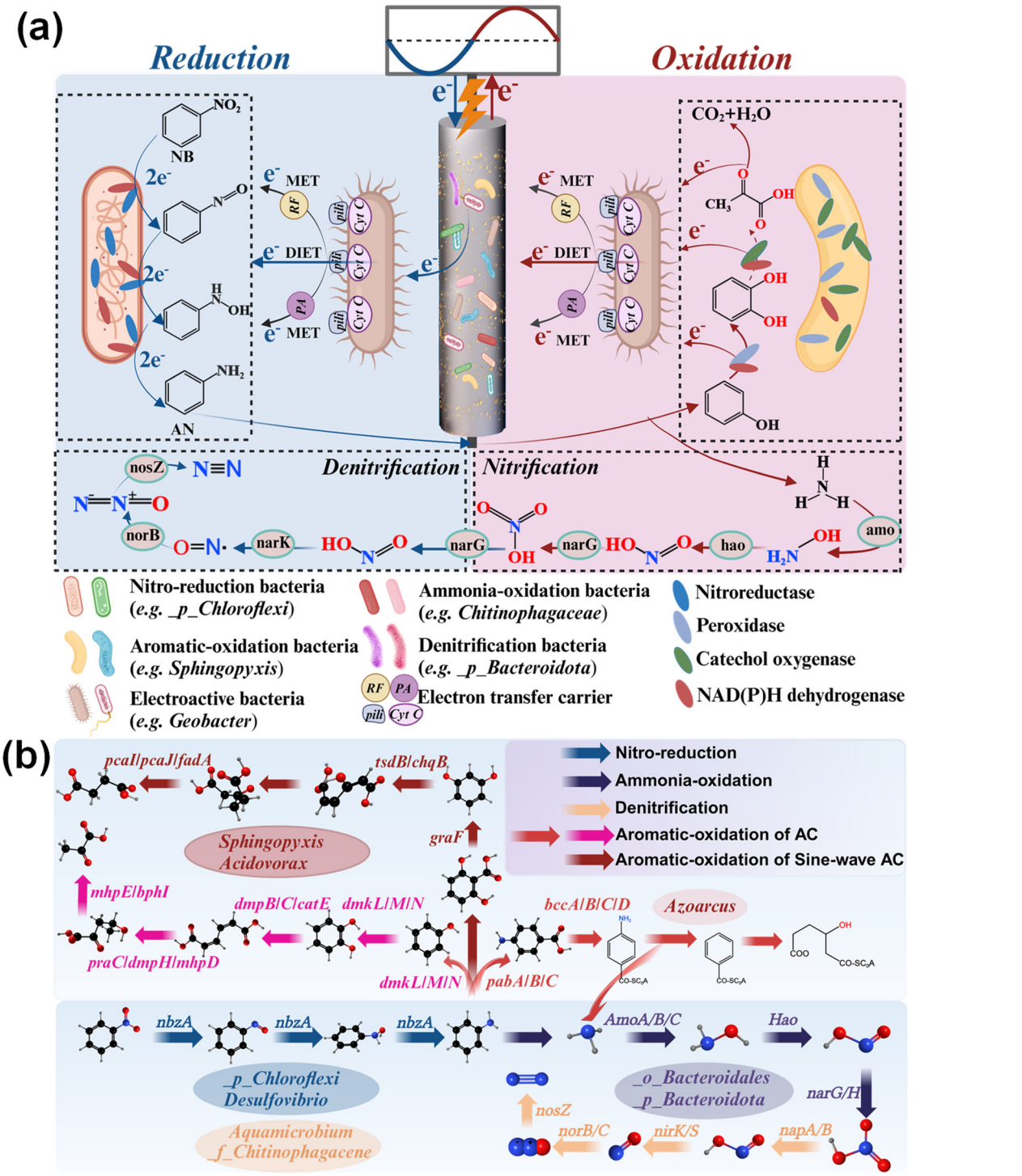

Fig. 7 | A mechanistic model for AC-driven redox in efficient mineralization of RONCs. a Conceptual model illustrating the working mechanism; (**b**) proposed metabolic pathways for NB degradation based on AC-driven redox processes.

Environmental Implications

The sine-wave AC-driven microbial redox process demonstrated superior efficiency in mineralizing RONCs (e.g., NB), outperforming square-wave AC and DC processes in NB reduction, intermediate oxidation, and TN removal. Energy consumption ranked as sine-wave AC (6.22 $W{\cdot}h{\cdot}L_{reactor}^{-1}$) <square-wave AC (7.50 $W{\cdot}h{\cdot}L_{reactor}^{-1}$) < DC (8.00 $W{\cdot}h{\cdot}L_{reactor}^{-1}$). AC-stimulated biofilms exhibited enhanced electron utilization and transfer, increased catalytic activity, and greater biofilm thickness, underscoring its integrated bioredox functions, bidirectional electron transfer capabilities, and charge-discharge properties. AC stimulation fostered a synergistic microbiome optimized for NB metabolism, enriched with functional consortia proficient in NB reduction, aromatic intermediate oxidation, ammonia oxidation, nitrate/nitrite reduction, and electron transfer. This collaborative microbiome showed a significant enrichment of functional genes encoding nitroreductases, catechol dioxygenase, ammonia monooxygenase, nitrate/nitrite reductases, and redox mediator proteins. Metatranscriptomics analysis revealed upregulation of genes related to ribosome function and carbon metabolism, crucial for energy and electron transport in the sine-wave AC-driven bioelectrode. Additionally, metabolomics analysis indicated an increase in metabolites associated with NB

metabolism, confirming the sine-wave AC-driven bioelectrode's significant advantages in RONC mineralization. Notably, this study employed characterization strategies such as metagenomics, metatranscriptomics, and non-targeted metabolomics, combined with electrochemical analyses, to indirectly analyze EET pathways. Advancements in microbial metabolite isolation and purification, trace compound detection technologies, and microsensor techniques hold the potential to enable direct measurement of intermediate species and enzyme activity, as well as real-time monitoring of redox mediator cycling between oxidation and reduction phases. These innovations would significantly enhance the reliability and depth of insights into EET mechanisms.

Methods

Construction, acclimation and operation of AC bioelectrodes

A schematic diagram illustrating the construction of the AC bioelectrode is presented in Supplementary Fig. 13. Based on the design of a dual-chamber electrochemical reactor, the working electrode was precisely engineered as an AC bioelectrode. A function generator (model SDG2000X, Shenzhen Dingyang Technology Co., Ltd., China) was employed to adjust waveforms and control voltage, ensuring stable operation of sine- and square-wave AC bioelectrodes. A DC power supply (model MS152D, Dongguan Maihao Electronic Technology Co., Ltd., China) maintained the stable operation of the DC bioelectrode. All potentials were referenced to a saturated calomel electrode (SCE). Each reactor consisted of two chambers with a working volume of 110 mL, which were separated by a proton exchange membrane (PEM, N212, Dupont, U.S.). Two graphite brushes (3 cm diameter × 3 cm height, Haote New Material Co. Ltd., China) were used as the working electrode and counter electrode. The graphite brushes were pretreated with 1 M of HCl for 24 h and then immersed in the deionized water for another 24 h. Before application, the graphite brushes were calcinated with a muffle furnace (SX2–12–12A, Shaoxing Jiaxing Instrument Manufacturing Co., Ltd., China) at 450 °C for 30 min. Titanium wires (0.3 mm diameter, TA2, Taizhou Rongge Hardware Products Co., Ltd., China) connected the electrodes to form external circuits. The seed sludge for electrode biofilm inoculation was sourced from ChengDong WWTP (Yancheng, China), then filtered through a mesh and aerated N_2 aeration. The concentration of NB was set at ~60 mg/L in the working chamber to reflect typical wastewater conditions, consistent with prior studies[26]. In the counter chamber, potassium ferrocyanide $K_4Fe(CN)_6$ was used as the electron mediator. The detailed composition of the electrolytes and their pre-treatment methods are provided in Supplementary Table 4.

Four sets of bioelectrodes were operated under the specific parameters outlined in Supplementary Table 5. One set of bioelectrodes was driven by sine-wave AC (peak voltage (V_{peak}) = 0.7 V and −0.7 V; frequency = 0.83 mHz, polarity switching every 10 min). Another set was driven by square-wave AC (voltage = 0.5 V and −0.5 V; frequency = 0.83 mHz, polarity switching every 10 min). Additionally, one set of bioelectrodes was powered by a constant DC voltage of −0.5 V, while the final set operated under open-circuit condition. The voltage waveforms for the four electrical modes are shown in Fig. 1a. The effective value (root-mean-square voltage, V_{rms}) of sine-wave AC was 0.5 V ($V_{peak}/\sqrt{2}$)[53], corresponding to an equivalent power output of both a square-wave AC of 0.5 V and a DC voltage of 0.5 V. The DC voltage of −0.5 V was selected for its demonstrated efficacy in NB reduction[48]. Each working chamber was inoculated with 100 mL of fresh sludge mixture (10 mL seed sludge, 90 mL electrolyte) and stirred at 250 rpm for 5 days to promote biofilm development. The electrolyte solution was refreshed three times to enhance biofilm stabilization. Reactor startup was deemed successful upon achieving stable removal of NB and TOC across five batches. All experiments were conducted in triplicate at 25 ± 2°C.

Analytical methods and calculations

Water samples from the working chambers were first filtered using a 0.22 μm filter (Shanghai Xingya Material Co. Ltd., China). The concentrations of nitrobenzene (NB) and aniline (AN) were determined using high performance liquid chromatography (HPLC, 1260 Infinity II, Agilent, USA) equipped with a ZORBAX SB-C18 column (5 μm, 4.6 × 150 mm). The mobile phase consisted of methanol/water mixture (50:50, v/v) at a flow rate of 1.0 mL/min, with the column temperature maintained at 40°C, and an injection volume of 10 μl. Detection wavelengths of 254 nm and 288 nm were selected for the quantitative analysis of NB and AN, respectively[54]. The limit of detection (LOD), defined as the signal-to-noise ratio of 3, was 0.2 ppm for NB and 0.1 ppm for AN. The recovery rates for NB and AN were 97.6% and 96.4%, respectively. The relative standard deviations of the measured concentrations for both NB and AN were below 1.5%. Degradation products of NB were identified using gas chromatography-mass spectrometry (GC-MS) (TRACE 1300, Thermo Fisher Scientific Co., Ltd., USA) coupled with a flame ionization detector and a TG-5 column (30 m × 0.32 mm × 0.25 μm, Thermo Fisher Scientific Co., Ltd., USA). TOC was quantified using a TOC analyzer (MultiN/C2100, Analytik Jena AG, GER). TN, NH_4^+, NO_3^-, and NO_2^- were measured using a spectrophotometer (UV-1100, Mapada, China) following standard methods (APHA, 2012)[55]. CV and EIS were conducted on an electrochemical workstation (CHI660D, Chenhua Instruments Co. Ltd., China). CV scans were performed at 1 mV/s from −0.8 V to +0.8 V. EIS was conducted over frequencies ranging from 0.001 Hz to 10000 Hz at 1 mV, with data presented as Nyquist plots. The Randles model was selected as the equivalent circuit to describe biological systems with active electrochemical characteristics[56]. Based on Nyquist plots, the impedance was controlled by electron transfer process (high frequency semicircle) and diffusion process (low frequency ray). Randles model including ohmic resistance (R_s), charge transfer resistance (R_{ct}), boundary layer (W), and capacitance (CPE) has been used to describe electron transfer and diffusion processes[57]. EIS data were fitted to the Randles model using ZView software (version 3.2)[58], with error estimates below 5% for diffusive components and below 1% for resistive and capacitive elements. Alternative electrochemical models, including the Warburg and Gerischer models, were compared to the Randles model through literature analysis and practical validation[59,60]. Simulations using ZView software revealed that these alternative models yielded errors exceeding 20% for resistive and capacitive elements, underscoring the superior accuracy of the Randles model for this system. Electrode biofilm morphology was assessed via SEM (Nova NanoSEM 450, FEI, USA) and CLSM (LSM900, Carl ZEISS AG, GER) with DNA staining using a Calcein-AM/PI Kit (G1707-100T, Wuhan Saiweier Biotechnology Co., Ltd, China). The effective AC current value (I_{EVA}/I_{EVB}), the effective AC current density (J_{EV}) and EUE were calculated using methods described by previous study[14]. NB removal efficiency (RE_{NB}, %), accumulation ratio of intermediate products (AR, %), degradation efficiency of intermediate products (DE_{AN}, %), and TOC removal efficiency (RE_{TOC}, %) were calculated using Eq. 1, Eq. 2, Eq. 3, and Eq. 4, respectively. NB and TOC removal kinetics were fit by the apparent first-order and second-order reaction model using Eq. 5 and Eq. 6. Energy consumption (EC) and current density (J, mA/cm^2) was calculated using Eq. 7 and Eq. 8.

$$RE_{NB} = (C_0 - C_t)/C_0 \times 100\% \quad (1)$$

$$AR = C_{AN}/(C_0 - C_t) \times 100\% \quad (2)$$

$$DE_{AN} = 100\% - \mathrm{AR} \quad (3)$$

$$RE_{TOC} = (C_{0-\mathrm{TOC}} - C_{t-TOC})/C_{0-\mathrm{TOC}} \times 100\% \quad (4)$$

$$C_{tX} = C_{0X}e^{-kt} \quad (5)$$

$$C_{tX} = C_{0X}\left(1 - e^{-kt}\right) \quad (6)$$

$$EC = (P \times t)/\left(V \times \log\frac{C_0}{C_t}\right) \quad (7)$$

$$J = I/S \quad (8)$$

where t represents the reaction time (h), C_0 represents the initial NB concentration (mg/L), C_t represents the NB concentration (mg/L) at time t (h), C_{AN} represents the concentration (mg/L) of AN at time t (h), C_{0-TOC} represents the initial TOC concentration (mg/L), C_{t-TOC} represents the TOC concentration (mg/L) at time t (h), C_{tX} represents the NB/TOC concentrations (mg/L) at time (d), C_{0X} represents the initial NB/TOC concentrations (mg/L), k represents rate constant (d^{-1}), P (W) represents the power, V (L) represents the volume of the reactor. I (mA) represents current, S (cm^2) represents cross-sectional area of conductor.

Multi-omics sequencing analysis of electromicrobiome

Biofilm samples from all bioelectrodes were collected after the experiments for metagenomics, metatranscriptomics, and non-targeted metabolomics analyses. The raw high-throughput sequencing data of the electromicrobiome have been uploaded to NCBI's Sequence Read Archive (Accession: PRJNA1173498). Metagenomic analysis was conducted using shotgun sequencing performed by Shanghai Majorbio Biological Technology Co. Ltd. DNA extracted from environmental samples was fragmented (~350 bp), quality-checked via agarose gel electrophoresis, and prepared into paired-end libraries with ligated adapters. Sequencing on the Illumina HiSeq 2000 platform enabled microbial community profiling through species annotation and non-redundant TPM quantification[61].

In metatranscriptomics, the various functional genes were compared with each database for species annotation and abundance characterization of functional microorganisms. In the sequencing experiment, the sequences in each sample were introduced with an Index tag indicating the source information of the sample. The data of each sample was distinguished according to the Index sequence, and the extracted data was saved in fastq format. Use the software fastp (https://github.com/OpenGene/fastp) to cut the adapter sequence at the 3' end and the 5' end, and retain high-quality pair-end reads and single-end reads. Using software SortMeRNA (http://bioinfo.lifl.fr/RNA/sortmerna/), read aligned SILVA SSU (16S/18S) to SILVA LSU (23S/28S) database to remove rRNA reads. After obtaining high-quality reads, all sequencing reads need to be assembled. This analysis was the basis for subsequent processing and biological function analysis. Trinity (http://trinityrnaseq.github.io/) was a relatively authoritative software suitable for the assembly of Illumina short fragment sequences. This software selected transcripts with a length of greater than or equal to 300 bp. Gene expression levels were quantified by FPKM values using the KEGG database (https://www.genome.jp/kegg/).

Non-targeted metabolomics profiling was conducted using an LC-MS/MS system, capturing mass spectrometry signals in both positive and negative ion scanning modes across a mass-to-charge range of 70–1050 m/z. The frozen tissue grinding instrument was grinded for 6 min (-10 °C, 50 Hz). After centrifugation for 15 min (13000 g, 4 °C), the supernatant was transferred to a vial with intubating tube for analysis. In addition, 20 µL of supernatant was removed from each sample and mixed as a quality control sample. The chromatographic column was ACQUITY UPLC HSS T3 (100 mm × 2.1 mm i.d., 1.8 µm, Waters, Milford, USA). Mobile phase A was 95% water + 5% acetonitrile (containing 0.1% formic acid). Mobile phase B was 47.5% acetonitrile + 47.5%. Isopropanol + 5% water (containing 0.1% formic acid), injection volume of 3 µL, column temperature of 40 °C. All omics data were processed using the Majorbio Cloud Platform (https://cloud.majorbio.com).

Data availability

All data generated or analyzed during this study are included in this published article and its supplementary information file.

Received: 19 September 2024; Accepted: 13 January 2025;
Published online: 21 January 2025

References

1. Zhu, C., Huang, H. & Chen, Y. Recent advances in biological removal of nitroaromatics from wastewater. *Environ. Pollut.* **307**, 119670 (2022).
2. Sathiyan, G. et al. Recent progress in triazine-based fluorescent probes for detecting hazardous nitroaromatic compounds. *J. Environ. Chem. Eng.* **12**(3), 112804 (2024).
3. Shi, K. et al. Regulating microbial redox reactions towards enhanced removal of refractory organic nitrogen from wastewater. *Water Res.* **258**, 121778 (2024).
4. Gupta, S. & Ronen, Z. Biological treatment of nitroaromatics in wastewater. *Water* **16**(6), 901 (2024).
5. Yang, K., Abu-Reesh, I. M. & He, Z. Enhancing the degradation of selected recalcitrant organic contaminants through integrated cathode and anode processes in microbial electrochemical systems: a frontier review. *J. Hazard. Mater. Lett.* **3**, 100057 (2022).
6. Lin, B. et al. Evolution of aniline degradation and nitrogen removal performance in electro-enhanced sequence batch reactor under salinity stress: sludge characteristics and microbial diversity. *Environ. Pollut.* **334**, 122201 (2023).
7. Skouteris, G. et al. The use of pure oxygen for aeration in aerobic wastewater treatment: a review of its potential and limitations. *Bioresource. Technol.* **312**, 123595 (2020).
8. Yang, Y. et al. Performance of alternating-current-enhanced anaerobic membrane bioreactor: membrane fouling, wastewater treatment, and CH_4 production. *ACS Sustainable Chem. Eng.* **9**(47), 15973–15982 (2021).
9. Zhi, Z. et al. Bioelectrochemical regulation accelerates biomethane production from waste activated sludge: Focusing on operational performance and microbial community. *Sci. Total Environ.* **814**, 152736 (2022).
10. Yuan, Y. et al. Intermittent electric field stimulated reduction-oxidation coupled process for enhanced azo dye biodegradation. *Chem. Eng. J.* **451**, 138732 (2023).
11. Xie, F. et al. Exploring the potential of a novel alternating current stimulated iron-carbon anammox process: a new horizon for nitrogen removal. *Sci. Total Environ.* **912**, 168893 (2024).
12. Ahmadi, S. & Rezaee, A. Environmental pollution removal using electrostimulation of microorganisms by alternative current. *Enzyme Microb, Tech* **174**, 110369 (2024).
13. Hoseinzadeh, E., Rezaee, A. & Farzadkia, M. Nitrate removal from pharmaceutical wastewater using microbial electrochemical system supplied through low frequency-low voltage alternating electric current. *Bioelectrochemistry* **120**, 49–56 (2018).
14. Yuan, Y. et al. In situ coupling of reduction and oxidation processes with alternating current driven bioelectrodes for efficient mineralization of refractory pollutants. *Engineering* **43**, 125–138 (2024).
15. Yuan, Y. et al. Frequency-modulated alternating current-driven bioelectrodes for enhanced mineralization of Alizarin Yellow R. *J. Hazard. Mater.* **475**, 134906 (2024).
16. Sanchez, C., Dessi, P., Duffy, M. & Lens, P. N. L. Microbial electrochemical technologies: Electronic circuitry and characterization tools. *Biosens. Bioelectron.* **150**, 111884 (2020).
17. He, J. et al. Evaluating the influence of gradient applied voltages on electro-enhanced sequence batch reactor treating aniline wastewater: System performance, microbial community and functional genes. *J. Clean. Prod.* **389**, 136077 (2023).
18. Peng, H. J. et al. A metagenomic view of how different carbon sources enhance the aniline and simultaneous nitrogen removal capacities in the aniline degradation system. *Bioresour. Technol.* **335**, 125227 (2021).
19. Dehghani, S., Rezaee, A. & Hosseinkhani, S. Biostimulation of heterotrophic-autotrophic denitrification in a microbial

electrochemical system using alternating electrical current. *J. Clean. Prod.* **200**, 1100–1110 (2018).
20. Buzzetti, P. et al. Hollow bioelectrodes based on buckypaper assembly. Application to the electroenzymatic reduction of O_2. *Nanomater.* **12**(14), 2399 (2022).
21. Jamaludin, N. et al. Effect of pH, temperature and agitation on thermophilic biohydrogen production using immobilized cells on carbon composites (GAC-$NiFe_3O_4$). *Chem. Eng. J.* **485**, 149980 (2024).
22. Hayta, E. et al. Bacterial materials: applications of natural and modified biofilms. *Adv. Mater. Interfaces* **8**(21), 2101024 (2021).
23. Zhang, X., Prevoteau, A., Louro, R. O. & Paquete, C. M. Periodic polarization of electroactive biofilms increases current density and charge carriers concentration while modifying biofilm structure. *Biosens. Bioelectron.* **121**, 183–191 (2018).
24. Cai, W. et al. Quorum sensing alters the microbial community of electrode-respiring bacteria and hydrogen scavengers toward improving hydrogen yield in microbial electrolysis cells. *Appl. Energy* **183**, 1133–1141 (2016).
25. Li, C. et al. Insight into the Pseudocapacitive behavior of electroactive biofilms in response to dynamic-controlled electron transfer and metabolism kinetics for Current generation in water treatment. *Environ. Sci. Technol.* **57**(48), 19891–19901 (2023).
26. Qi, M. et al. Effects of surface charge, hydrophilicity and hydrophobicity on functional biocathode catalytic efficiency and community structure. *Chemosphere* **202**, 105–110 (2018).
27. Chen, H. Y. et al. Stimulation of oxygen to bioanode for energy recovery from recalcitrant organic matter aniline in microbial fuel cells (MFCs). *Water Res.* **81**, 72–83 (2015).
28. Wang, B., Liu, W., Zhang, Y. & Wang, A. Bioenergy recovery from wastewater accelerated by solar power: intermittent electro-driving regulation and capacitive storage in biomass. *Water Res.* **175**, 115696 (2020).
29. Lim, S. S. et al. Impact of applied cell voltage on the performance of a microbial electrolysis cell fully catalysed by microorganisms. *Int. J. Hydrogen Energy* **45**, 2557–2568 (2020).
30. Liang, D. et al. Construction of bidirectional electron transfer biofilms via periodic polarity reversal. *Chem. Eng. J.* **452**, 139145 (2023).
31. Liang, Z. et al. Enforcing energy consumption promotes microbial extracellular respiration for xenobiotic bioconversion. *Environ. Microbiol.* **25**(12), 2943–2957 (2023).
32. Gupta, S. et al. Transformation of 2, 4, 6-trinitrotoluene by *Stenotrophomonas* strain SG1 under aerobic and anaerobic conditions. *Chemosphere* **311**, 137085 (2023).
33. Wu, L. et al. Cooperation between partial-nitrification, complete ammonia oxidation (comammox), and anaerobic ammonia oxidation (anammox) in sludge digestion liquid for nitrogen removal. *Environ. Pollut.* **254**, 112965 (2019).
34. Guo, W. et al. Interspecies electron transfer between *Geobacter* and denitrifying bacteria for nitrogen removal in bioelectrochemical system. *Chem. Eng. J.* **455**, 139821 (2023).
35. Yun, H. et al. Response of anodic bacterial community to the polarity inversion for chloramphenicol reduction. *Bioresource Technol.* **221**, 666–670 (2016).
36. Verma, H. et al. Comparative genomics of *Sphingopyxis* spp. unravelled functional attributes. *Genomics* **112**(2), 1956–1969 (2020).
37. Zheng, M. et al. Metagenomic analysis of aromatic ring-cleavage mechanism in nano-Fe_3O_4@activated coke enhanced bio-system for coal pyrolysis wastewater treatment. *J. Hazard. Mater.* **414**, 125387 (2021).
38. Su, H. et al. Unraveling the effects of light rare-earth element (Lanthanum (III)) on the efficacy of partial-nitritation process and its responsible functional genera. *Chem. Eng. J.* **408**, 127311 (2021).
39. Wu, N. et al. Understanding the impacts of intermittent electro field on the bioelectrochemical aniline degradation system: performance, microbial community and functional enzyme. *Environ. Res.* **231**, 116039 (2023).
40. Chen, D. et al. Simultaneous debromination and mineralization of bromophenol in an up-flow electricity-stimulated anaerobic system. *Water Res.* **157**, 8–18 (2019).
41. Boddu, R. S., Perumal, O. & Divakar, K. Microbial Nitroreductases: A versatile tool for biomedical and environmental applications. *Biotechnol. Appl. Bioc.* **68**(6), 1518–1530 (2021).
42. Lehtovirta-Morley, L. E. Ammonia oxidation: ecology, physiology, biochemistry and why they must all come together. *FEMS. Microbiol. Lett.* **365**(9), 058 (2018).
43. Trotter, V. V. et al. Large-scale genetic characterization of the model sulfate-reducing bacterium, *Desulfovibrio* vulgaris Hildenborough. *Front. Microbiol.* **14**, 1095191 (2023).
44. Zhao, Z., Zhao, Y. & Marotta, F. The microbial community structure and nitrogen cycle of high-altitude pristine saline lakes on the Qinghai-Tibetan plateau. *Front. Microbiol.* **15**, 1424368 (2024).
45. Cao, Q. et al. Compartmentation of microbial communities in structure and function for methane oxidation coupled to nitrification-denitrification. *Bioresource Technol.* **341**, 125761 (2021).
46. Surti, P., Kailasa, S. K. & Mungray, A. K. Genetic engineering strategies for performance enhancement of bioelectrochemical systems: a review. *Sustain. Energy Techn.* **47**, 101732 (2021).
47. He, Y. et al. Deciphering the potential role of quorum quenching in efficient aerobic denitrification driven by a synthetic microbial community. *Water Res.* **251**, 121162 (2024).
48. Yang, K. et al. Bioelectrochemical degradation of monoaromatic compounds: current advances and challenges. *J. Hazard. Mater.* **398**, 122892 (2020).
49. Mou, B., Gong, G. & Wu, S. Biodegradation mechanisms of polycyclic aromatic hydrocarbons: combination of instrumental analysis and theoretical calculation. *Chemosphere* **341**, 140017 (2023).
50. Bertato, L., Chirico, N. & Papa, E. Predicting the bioconcentration factor in fish from molecular structures. *Toxics* **10**(10), 581 (2021).
51. AlSayed, A., Soliman, M. & Eldyasti, A. Microbial fuel cells for municipal wastewater treatment: from technology fundamentals to full-scale development. *Renew. Sust. Energ. Rev.* **134**, 110367 (2020).
52. Park, J. G., Jiang, D. Q., Lee, B. & Jun, H. B. Towards the practical application of bioelectrochemical anaerobic digestion (BEAD): Insights into electrode materials, reactor configurations, and process designs. *Water Res.* **184**, 116214 (2020).
53. Gilmore, J. et al. Assessing the importance of the root mean square (RMS) value of different waveforms to determine the strength of a dielectrophoresis trapping force. *Electrophoresis* **38**(20), 2561–2564 (2017).
54. Xia, Y. et al. Enhanced anaerobic reduction of nitrobenzene at high salinity by betaine acting as osmoprotectant and regulator of metabolism. *Water Res.* **223**, 118982 (2022).
55. APHA. *Standard Methods for the Examination of Water and Wastewater.* https://www.standardmethods.org/ (2012).
56. Torres-Rojas, F. et al. Bioelectrochemical chlorate reduction by Dechloromonas agitata CKB. *Water Res.* **315**, 123818 (2020).
57. Zhao, S. et al. Elevated Cr(VI) reduction in a biocathode microbial fuel cell without acclimatization inversion based on strain Corynebacterium vitaeruminis LZU47-1. *Int. J. Hydrogen Energ.* **46**(4), 3193–3203 (2021).
58. Shi, H. et al. Simultaneous high-concentration pyridine removal and denitrification in an electricity assisted bio-photodegradation system. *Chem. Eng. J.* **430**, 132598 (2022).
59. Cruz-Manzo, S. & Greenwood, P. Study of oxygen diffusion in the cathode catalyst layer and gas diffusion layer for polymer electrolyte fuel cells with EIS. *J. Electroanal. Chem.* **892**, 115270 (2021).
60. Cariati, L. S. & Buoro, R. M. Evaluation of ionic natural deep eutectic solvents (NADES) modified binders towards the chemical properties of carbon paste electrodes. *Electrochem. Commun.* **109**, 106605 (2019).

61. Bi, Q. et al. Pharmacological and metagenomics evidence of polysaccharide from *Polygonum multiflorum* in the alleviation of insulin resistance. *Int. J. Biol. Macromol.* **164**, 1070–1079 (2020).

Acknowledgements

This work was supported by the National Natural Science Foundation of China (NSFC, Grant No. 52170054, 51608467 and 52200202); by Qinghai Science and Technology Department Project (No. 2022-ZJ-923); by 'Qing Lan Project' of Colleges and Universities in JiangSu Province; and by the Graduate Research Innovation Program of Yancheng Institute of Technology (KYCX24_XZ026).

Author contributions

Y.Y. and X.Q. contributed equally to this work. All authors have provided substantial contributions to the conception or design of the work or analysis drafted the work or revised it critically for important intellectual content, have approved of the completed version, and are accountable for all aspects of the work in ensuring that questions related to the accuracy or integrity of any part of the work are appropriately investigated and resolved.

Competing interests

The authors declare no competing interests.

Additional information

Supplementary information The online version contains supplementary material available at https://doi.org/10.1038/s41545-025-00439-5.

Correspondence and requests for materials should be addressed to Yang Liu or Fan Chen.